Bioconjugate Chemistry

pubs.acs.org/bc Article

# Bioconjugate Supramolecular $Pd^{2+}$ Metallacages Penetrate the Blood Brain Barrier *In Vitro* and *In Vivo*

Ben Woods,[¶] Rúben D. M. Silva,[¶] Claudia Schmidt, Darren Wragg, Marco Cavaco, Vera Neves, Vera F. C. Ferreira, Lurdes Gano, Tânia S. Morais, Filipa Mendes,* João D. G. Correia,* and Angela Casini*

Cite This: *Bioconjugate Chem.* 2021, 32, 1399−1408 Read Online

ACCESS | Metrics & More | Article Recommendations | Supporting Information

**ABSTRACT:** The biomedical application of discrete supramolecular metal-based structures, specifically self-assembled metallacages, is still an emergent field of study. Capitalizing on the knowledge gained in recent years on the development of 3-dimensional (3D) metallacages as novel drug delivery systems and *theranostic* agents, we explore here the possibility to target $[Pd_2L_4]^{4+}$ cages (L = 3,5-bis(3-ethynylpyridine)phenyl ligand) to the brain. In detail, a new water-soluble homoleptic cage ($C^{PepH3}$) tethered to a blood brain barrier (BBB)-translocating peptide was synthesized by a combination of solid-phase peptide synthesis (SPPS) and self-assembly procedures. The cage translocation efficacy was assessed by inductively coupled mass spectrometry (ICP-MS) in a BBB cellular model *in vitro*. Biodistribution studies of the radiolabeled cage $[[^{99m}TcO_4]^- \subset C^{PepH3}]$ in the CD1 mice model demonstrate its brain penetration properties *in vivo*. Further DFT studies were conducted to model the structure of the $[[^{99m}TcO_4]^- \subset$ cage] complex. Moreover, the encapsulation capabilities and stability of the cage were investigated using the $[ReO_4]^-$ anion, the "cold" analogue of $[^{99m}TcO_4]^-$, by $^1H$ NMR spectroscopy. Overall, our study constitutes another proof-of-concept of the unique potential of supramolecular coordination complexes for modifying the physiochemical and biodistribution properties of diagnostic species.

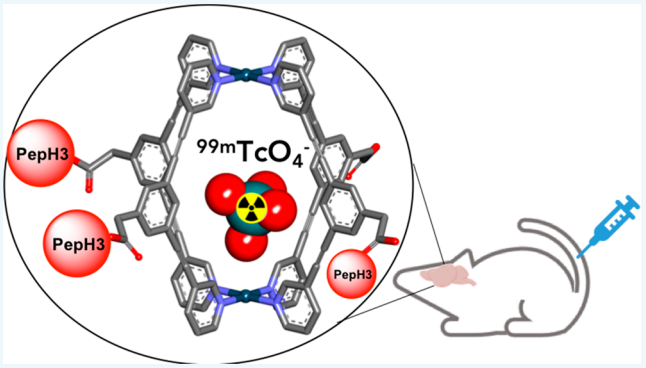


## INTRODUCTION

The understanding of pathophysiological mechanisms of brain diseases such as central nervous system (CNS) disorders (e.g., Alzheimer's and Parkinson's diseases) and malignant brain tumors has improved considerably in the past few years, in parallel with great advances in medical technology.[1] However, most brain diseases remain poorly treated, as the development of innovative drugs targeting the brain is rather challenging. Indeed, the failure rate for new CNS-targeted drugs is high compared to most other therapeutic areas of drug discovery, which is mainly related to the low permeability of the blood-brain barrier (BBB). Similarly, the ability to image structure and function in the brain using different imaging modalities holds the promise of providing insight into pathophysiological conditions, but is greatly limited by the possibility to deliver contrast and imaging agents with molecular specificity across the BBB.

The BBB is a tightly regulated barrier between systemic circulation and the brain that behaves as a careful guardian of this organ, preventing foreign substances such as toxins, but also therapeutic small molecules or biotherapeutics, from entering the brain. This issue arises from the specific anatomical and functional features of the BBB, where a complex interplay between microvascular endothelial cells firmly sealed with tight junctions, astrocytes, pericytes, basal lamina, and extracellular matrix takes place.[2,3] In addition, brain capillary endothelial cells express efflux transport systems that remove undesirable substances from the brain to the systemic circulation, reinforcing the "shielding" properties of the BBB.

With this physiological scenario taken into consideration, there is an urgent need for innovative and efficient technologies for delivering target-specific drugs and/or imaging agents across the BBB for the effective treatment and diagnosis of brain diseases. Aimed at addressing simultaneously issues related to drug localization, drug release, and drug efficacy, multicomponent constructs in which drugs and imaging agents are combined in molecular or nanosized platforms, named *theranostic agents*, have been explored in recent years.[4−7] This

**Special Issue:** State-of-the-Art of Radiometal-based Bioconjugates for Molecular Imaging and Radiotherapy

**Received:** December 1, 2020
**Revised:** December 28, 2020
**Published:** January 13, 2021







https://dx.doi.org/10.1021/acs.bioconjchem.0c00659
*Bioconjugate Chem.* 2021, 32, 1399−1408

**Scheme 1. (A) Synthesis of the Bioconjugated Ligand $L^{PepH3}$ *via* Solid Phase Synthesis and (B) Full Structure of the $L^{PepH3}$ Peptide**

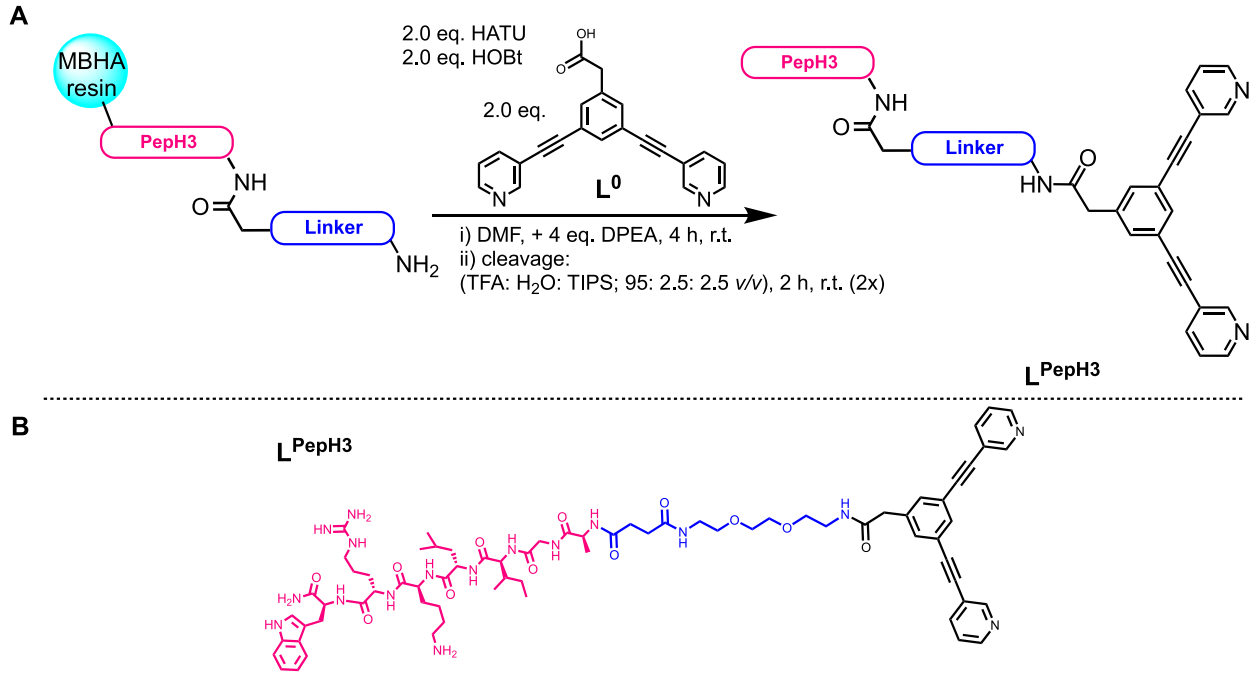


approach, which can include *in vivo* molecular neuroimaging, is expected to significantly improve the management of poorly treated brain diseases, namely, brain cancer. Indeed, it is widely accepted that the design of highly versatile targeted *theranostic* delivery systems needs to be further studied and explored to enlarge the toolbox of strategies for treatment, diagnosis, and monitoring of brain diseases.

Various possible strategies for transporting drugs of different nature across the BBB, other than the invasive approach including BBB disruption, have been explored depending on the type of molecules or systems considered.[8] For example, recent studies to deliver drugs and or/imaging agents (e.g., gadolinium-containing complexes for magnetic resonance imaging (MRI)) to the brain include, among others, the use of viral vectors, nonviral nanoparticles, exosomes, or peptide-based delivery vectors.[5,6,9,10] The latter act as shuttles for drug delivery across the BBB, including large molecules such as antibodies or nanoparticles. Within this context, cell-penetrating peptides (CPPs), which are short peptide sequences that may present cationic, amphipathic, or hydrophobic properties, are highly efficient shuttles.[11−13]

In the last decades, three-dimensional (3D) Supramolecular Coordination Complexes (SCCs), with suitable metal centers undergoing coordination-driven self-assembly with ligands containing multiple binding sites,[14,15] have received great attention in the biomedical context, including for biomolecular recognition, drug delivery, photodynamic therapy, and imaging.[16−19] The inspiration for the use of SCCs in biomedical applications arises from a number of key features, including: (i) the ease of fine-tuning the topological structures of the resulting coordination complexes; (ii) the plentiful choices of metal knots and ligands with changeable sizes and angles; and (iii) the feasible integration of functional groups via pre- or post-assembly modifications of the coordination building block. The latter is essential to design multimodal SCCs as targeted drug delivery systems and as *theranostic* agents.

Recently, the family of 3D SCCs named "metallacages" (also referred to as "capsules", "boxes", etc.) of general formula ($M_nL_m$)—where M is usually Pd(II), Pt(II), or half-sandwich organometallic clips based on Ru(II), Os(II), and Ir(III); and L is the ligand of the coordination complex—were particularly explored also due to their host−guest chemistry capability.[20−23] In fact, these discrete chemical entities feature a cavity able to firmly encapsulate small molecules, including ionic species. As an example, the cationic metallacages $[Pd_2L_4]^{4+}$ (L = 3,5-bis(3-ethynylpyridine)phenyl) were successfully explored by some of us as drug delivery systems for the anticancer drug cisplatin, whereby drug encapsulation minimizes its systemic toxicity while reducing its speciation in biological environment.[24] Structural studies by NMR spectroscopy and X-ray diffraction demonstrated encapsulation of two cisplatin molecules in the cage's cavity.[24,25] Afterward, the *exo*-functionalization of the ligand was exploited to include different linkers for tethering the metallacage to peptides via amide bond formation.[26] Thus, $[Pd_2L_4]^{4+}$ cages conjugated to four ligands selective for binding to integrins $\alpha v\beta 3$ or $\alpha 5\beta 1$ were studied for their integrin recognition properties using an ELISA assay, and were shown to maintain high binding affinity and selectivity.[27] Upon encapsulation, cisplatin showed increased cytotoxicity *in vitro* in melanoma A375 cells overexpressing $\alpha v\beta 3$ integrins. Of note, the cages and their building blocks did not show any toxic effect in healthy tissue slices *ex vivo*.[27]

In another example, Chen and Stang and co-workers developed a sophisticated porphyrin-based metallacage acting as a theranostic platform: not only did the metallacage show antitumor efficacy via a combination of chemotherapy and PDT treatments, but further labeling by a positron emitting radiometal ($^{64}Cu$) or a paramagnetic Mn ion, enabled excellent *in vivo* positron emission tomography (PET) imaging and MRI capabilities, respectively.[28] Concerning single-photon emission computed tomography (SPECT) imaging, using a kinetically robust tetrahedral $Co_4L_6$ (L = 5′-(4′-amino-(2,2′-bipyridin)-5-yl)-(2,2′-bipyridin)-4-amine) capsule, Lusby and Archibald and


https://dx.doi.org/10.1021/acs.bioconjchem.0c00659
Bioconjugate Chem. 2021, 32, 1399−1408

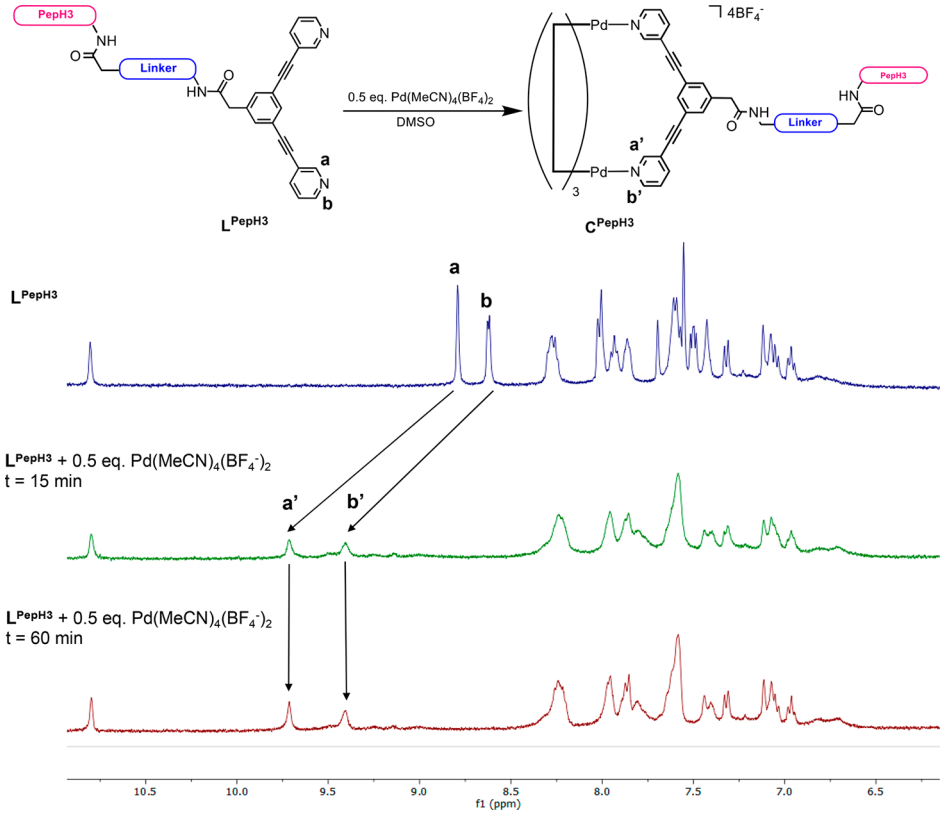


**Figure 1.** Scheme of the self-assembly of cage $\mathbf{C}^{\mathbf{PepH3}}$ and stacked $^1$H NMR spectra (DMSO-$d_6$) showing quantitative metallacage formation over 1 h. The process can be monitored by the disappearance of the ligand peaks a and b, and the emergence of the metallacage signals a′ and b′.

co-workers showed the feasibility of encapsulating the $\gamma$-emitting anion $[^{99m}TcO_4]^-$, which is the most widely used precursor for the preparation of radiopharmaceuticals in nuclear diagnostic imaging.[29] Noteworthy, SPECT imaging of the caged-anion revealed a marked change in the biodistribution of the host−guest system compared to the free oxo-anion, which accumulates in the thyroid, suggesting that the capsule remained intact *in vivo*. While further optimization is needed, including targeting to disease tissues, these results certainly move clinical applications of metallo-supramolecular species a step further.

Following these promising results, we decided to continue the investigation of self-assembled $[Pd_2L_4]^{4+}$ metallacages as possible versatile brain-targeted delivery systems, encapsulating the $[^{99m}TcO_4]^-$ anion as the imaging component and conjugating the cage to a BBB-translocating peptide (PepH3) shuttle. $[^{99m}TcO_4]^-$ was chosen to investigate the stability of the cage and its biodistribution *in vivo*. Moreover, the speed and efficacy of noncovalent encapsulation of pertechnetate, if achieved, provide an advantage over the classical *in situ* reduction of the +7 oxidation state to the +5 oxidation state, followed by metal complexation, necessary for SPECT imaging.

Concerning the selected targeting peptide, it was reported by some of us that short peptide sequences from the Dengue virus type-2 capsid protein (DEN2C) are able to translocate endothelial cells by receptor-independent routes. The most interesting peptide, PepH3, displayed a very good brain penetration both *in vitro* and *in vivo*.[30,31] Moreover, the ability of PepH3 to transport large cargos across the BBB was tested using a cellular *in vitro* BBB model which showed ca. 30% translocation of PepH3-conjugated green fluorescent protein (GFP) after 5 h.[32] PepH3 allowed efficient *in vivo* brain translocation of larger proteins such as antibody fragments (e.g., the anti-$\beta$-amyloid protein 42 single-domain antibody[33]).

Therefore, we report here on the synthesis of a new homoleptic Pd(II) cage *exo*-conjugated to PepH3 that was accomplished combining classical solid-phase peptide synthesis (SPPS) approaches with self-assembly procedures (see Experimental Section for details). The cage structure was confirmed by different analytical and spectroscopic techniques and its translocation efficacy was assessed in a BBB cellular model *in vitro*. Moreover, the encapsulation capabilities of the cage were investigated using the $[ReO_4]^-$ anion, the "cold" analogue of $[^{99m}TcO_4]^-$, by $^1$H NMR spectroscopy, as well as by density functional theory (DFT) studies. The stability of the $[[ReO_4]^- \subset \text{cage}]$ adduct was also evaluated in aqueous environment in the presence of GSH by $^1$H NMR spectroscopy. We also describe the radiolabeling of the cage with $[^{99m}TcO_4]^-$, the purification of the resulting radioactive cage, and the assessment of its brain penetration properties *in vivo* in CD1 mice.

## RESULTS AND DISCUSSION

**Synthesis of PepH3 Functionalized Ligand.** The shuttle peptide PepH3 was synthesized following standard fluorenylmethoxycarbonyl(Fmoc)-SPPS conditions in a microwave-assisted automated peptide synthesizer (CEM Liberty) using rink amide MBHA resin as previously reported[30] (see Experimental Section, SI, Figure S5). After assembly on the resin, the fully protected resin-bound PepH3 peptide was treated with a 20% piperidine solution in DMF to remove the Fmoc protecting group and conjugated to a Fmoc-protected N-terminal PEG spacer unit (1-(9*H*-fluoren-9-yl)-3,14-dioxo-2,7,10-trioxa-4,13-diazaheptadecan-17-oic acid, Fmoc-PEG2).


https://dx.doi.org/10.1021/acs.bioconjchem.0c00659
Bioconjugate Chem. 2021, 32, 1399−1408

Small-scale peptide cleavage from the resin was performed for analyses by Fmoc-deprotection with piperidine and using a standard cleavage cocktail solution (95% trifluoracetic acid (TFA), 2.5% water, 2.5% triisopropyl silane v/v). After removal of TFA under nitrogen stream, the peptide was analyzed by analytical RP-HPLC and electrospray ionization mass spectrometry (ESI-MS), which confirmed the presence of the PepH3-$(PEG)_2$-$NH_2$ conjugate (see SI, Figure S6).

In parallel, the carboxylic *exo*-functionalized ligand 2-(3,5-bis(pyridin-3-ylethynyl)phenyl)acetic acid ($\mathbf{L^0}$) was synthesized following previously reported procedures[25] and tethered to the fully protected resin bound PepH3-$(PEG)_2$-$NH_2$ conjugate, following N-terminal Fmoc removal, via amide bond formation under standard Fmoc-SPPS conditions (Scheme 1, see SI, Figures S1−S2). The conjugation was initially confirmed via the Kaiser test, which evidenced the absence of primary amine groups, suggesting complete conjugation of the ligand to the resin bound peptide-PEG moiety. Again, small-scale peptide deprotection and cleavage was performed, and separation by RP-HPLC, followed by ESI-MS analysis, confirmed formation of the PepH3-$(PEG)_2$-$\mathbf{L^0}$ conjugate ($\mathbf{L^{PepH3}}$). Then, the remaining resin with ($\mathbf{L^{PepH3}}$) was processed to remove the Fmoc group and the $\mathbf{L^{PepH3}}$ conjugate cleaved from the resin using the standard cleavage cocktail. After TFA removal by evaporation, the peptide solution was purified by preparative RP-HPLC and the collected fractions dried by lyophilization to yield the pure (>95%) PepH3 *exo*-functionalized ligand, $\mathbf{L^{PepH3}}$ (Scheme 1, Figures S3 and S7−S8)

**Self-Assembly of PepH3 Exo-functionalized $[Pd_2L_4]^{4+}$ Metallacage.** The $\mathbf{L^{PepH3}}$ conjugate was self-assembled into the corresponding $Pd_2L_4$ metallacage $\mathbf{C^{PepH3}}$ following the addition of tetrakis(acetonitrile)palladium(II)tetrafluoroborate (1:2; $Pd^{2+}$:$\mathbf{L^{PepH3}}$) in DMSO at room temperature (Figure 1). The successful self-assembly to the metallacage $\mathbf{C^{PepH3}}$ was monitored by $^1$H NMR spectroscopy in DMSO-$d_6$ over 1 h to ensure full coordination of the ligand, $\mathbf{L^{PepH3}}$, to the palladium centers. In Figure 1, the signals corresponding to $H_a$ and $H_b$ of $\mathbf{L^{PepH3}}$ ($\delta$ = 8.78 ppm and $\delta$ = 8.61 ppm, respectively) disappeared after 15 min, while two new peaks appeared that correspond to $H_a$ and $H_b$ of $\mathbf{C^{PepH3}}$ ($\delta$ = 9.61 ppm and $\delta$ = 9.42 ppm, respectively, a′ and b′ in Figure 1). Of note, the new metallacage features pronounced water solubility compared to the nonbioconjugate cage scaffold.[25]

**DFT Study of the Host−Guest Complex.** The host−guest complex featuring the cage scaffold encapsulating pertechnetate was further studied by DFT methods. Specifically, the optimized structure of the nontargeted cage $\mathbf{C^0}$[25] encapsulating the $[TcO_4]^-$ anion was obtained by DFT-PBE0[34] as described in the Experimental Section. The $[[^{99m}TcO_4]^- \subset \mathbf{C^0}]$ complex is reported in Figure 2 and shows a slight distortion of the cage structure and reorientation or the pertechnetate anion within the cavity, with one oxygen of the tetrahedral structure facing toward one of the two $Pd^{2+}$ ions (bottom $Pd^{2+}$ ion, Figure 2A). Of note, the anion migrates toward the latter $Pd^{2+}$ ion, rather than staying equidistant from both cations in the center of the cavity. This results in a TcO−Pd interatomic distance of 3.026 Å and TcO−CH distances of 2.292, 2.248, 2.275, and 2.316 Å, respectively (with C being the four carbons on the pyridyl rings in a′ position according to the NMR assignment, Figure 1). The total energy of the $[[^{99m}TcO_4]^- \subset \mathbf{C^0}]$ complex was calculated to be $-2.2 \times 10^{-17}$ kJ.

**Encapsulation Studies of Perrhenate.** To validate the host−guest chemistry of the targeted metallacage, we used $^1$H NMR spectroscopy and recorded the spectrum of $\mathbf{C^{PepH3}}$ in the presence of the "cold" analogue of pertechnetate, namely, perrhenate $[ReO_4]^-$. The binding of this anion is easy to observe due to slow exchange on the $^1$H NMR time scale. Upon addition of $[ReO_4]^-$ to the cage solution (see Experimental section for details), the $^1$H NMR spectra showed the upfield shifts of the $\alpha$-pyridinyl protons, indicating the successful encapsulation of perrhenate into the cage cavity. Figure 3 reports the spectrum of cage $\mathbf{C^{PepH3}}$ vs the one of the $[[ReO_4]^- \subset \mathbf{C^{PepH3}}]$ complex. The obtained results are in line with those previously reported on cobalt cages.[29] The stability of the cage−perrhenate complex was monitored in water, and buffered solution over 24 h by NMR spectra showed no variations even after freeze−thawing of the solution (data not shown). Furthermore, the stability of $[[ReO_4]^- \subset \mathbf{C^{PepH3}}]$ was evaluated in the presence of excess glutathione (GSH) by $^1$H NMR over 24 h (Figure S9, Supporting Information). In this case, cage disassembly occurred over time, and after 1 h incubation, a significant reduction of the signals corresponding to the aforementioned $\alpha$-pyridinyl protons took place. Based on these preliminary studies, we cannot exclude that partial disruption of the host−guest

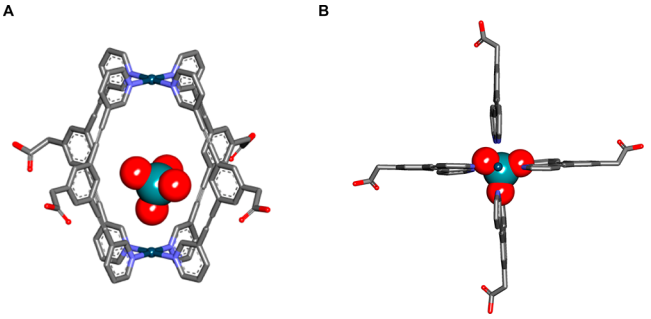


**Figure 2.** Optimized structure of the $\mathbf{C^0}$ cage encapsulating the $TcO_4^-$ anion, $[[^{99m}TcO_4]^- \subset \mathbf{C^0}]$, obtained by DFT methods. The cage is shown in stick representation and $TcO_4^-$ is shown in VDW representation (C = gray, N = light blue, O = red, Pd = dark blue, Tc = teal. Hydrogens omitted for clarity). (A) Side view showing the positioning of the anion within the $\mathbf{C^0}$ cage. (B) Top view showing the positioning of the anion within $\mathbf{C^0}$ and the slight distortion of the cage structure upon anion encapsulation. Figure generated using Discovery Studio Visualizer software.[35]

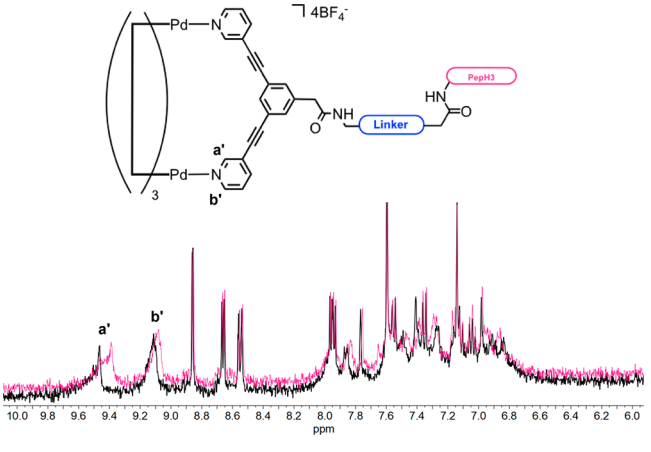


**Figure 3.** $^1$H NMR spectra (400 MHz, $D_2O$/DMSO-$d_6$, 298 K) of the free cage $\mathbf{C^{PepH3}}$ (black) and encapsulating perrhenate to form the $[[ReO_4]^- \subset \mathbf{C^{PepH3}}]$ complex (magenta), 30 min incubation after addition of $[ReO_4]^-$.


https://dx.doi.org/10.1021/acs.bioconjchem.0c00659
Bioconjugate Chem. 2021, 32, 1399−1408

system may occur also in the presence of serum components over time.

**Evaluation of the Metallacages in an In Vitro BBB Cell Model.** The evaluation of the ability of the metallacages $\mathbf{C}^{\mathbf{PepH3}}$ to translocate the BBB was performed in the bEnd.3 cell model *in vitro*, in comparison to the untargeted cage $\mathbf{C}^{\mathbf{0}}$.[25] From the different established cellular models of the BBB (excellently reviewed by Brodin and colleagues[36]), the murine brain endothelioma bEnd.3 cell line was selected due to its advantages, such as easy growth and low cost, the ability to maintain BBB characteristics over many passages, and the formation of functional barriers.[30,37] This immortalized cell line has been shown to express the tight junction proteins ZO-1, ZO-2, occludin, and claudin-5 as well as junctional adhesion molecules. The *in vitro* BBB model was realized by growing the bEnd.3 cells in fibronectin-coated transwell filters, enabling the establishment of a tight monolayer of cells (Figure 4A).

A

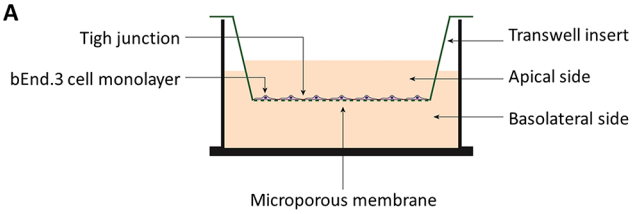


B

| | 2h | 5h |
|---|---|---|
| Ratio translocation $\mathbf{C}^{\mathbf{PepH3}}/\mathbf{C}^{\mathbf{0}}$ | 1.9 | 1.66 |

**Figure 4.** (A) Scheme of the *in vitro* BBB cellular model, grown on a transwell membrane system. (B) Ratio of BBB translocation values of the tested metallacages *in vitro*, recorded at different times.

Before the study of the metallacages and the evaluation of their ability to cross this BBB cell model, an initial evaluation of the integrity of the endothelial barrier was performed through the assessment of permeability of fluorescently labeled dextran (FD) with a 4 kDa molecular weight (FD4). Molecules such as FD4 should present a negligible translocation, and in the conditions used here, integrities in the range of 90−95% were detected (data not shown). Next, a cell viability assay was performed to confirm the nontoxicity of the metallacages in this cell line. It is worth mentioning that the correct self-assembly of the metallacage was validated prior to each experiment by $^{1}$H NMR spectroscopy in nondeuterated DMSO (data not shown) by the use of a capillary insert filled with a deuterated solvent which the NMR spectrometer can lock on. Although there is inevitably a large peak corresponding to the nondeuterated DMSO solvent molecules, as the proton peaks of the ligand are in the aromatic region (approximately 7−10 ppm), and the solvent signal maximum is approximately 2.50 ppm, the large DMSO solvent peak does not mask the proton signals of the ligand. As such, the self-assembly of $Pd_2L_4$ metallacages can be successfully monitored directly in nondeuterated DMSO, and this sample can then be immediately used for *in vitro* studies.

From this first evaluation, it is of note that for both cages $\mathbf{C}^{\mathbf{0}}$ and $\mathbf{C}^{\mathbf{PepH3}}$, as well as for the peptidic ligand, no significant cytotoxicity was observed, with $EC_{50} > 100\ \mu M$ (see Supporting Information Figure S10). These results are in line with the noncytotoxic profile previously described for the $Pd^{2+}$ precursor and the $\mathbf{C}^{\mathbf{0}}$ cage in human cancer cells[27] and for the peptide PepH3 in the bEnd3 cell model.[30]

To assess the ability of the metallacages to translocate the *in vitro* BBB model, bEnd3 cells were exposed to the metallacages for 2 and 5 h, respectively, and the Pd content in the apical and basolateral media was determined by inductively coupled plasma mass spectrometry (ICP-MS). The translocation efficiency was determined by the amount of Pd detected in the basolateral medium as a % of the total Pd content (apical + basolateral media). In Figure 4B, the ratio of translocation of $\mathbf{C}^{\mathbf{PepH3}}$ versus $\mathbf{C}^{\mathbf{0}}$ in correspondence to different incubation times (2 and 5 h, respectively) is presented. Overall, the ICP-MS determination of the Pd content showed that both cages are able to efficiently translocate the *in vitro* BBB cell model, although to a different extent, with $\mathbf{C}^{\mathbf{PepH3}}$ presenting the highest translocation values over time. The amount of Pd recovered in the apical and basolateral media was always >98% of the total applied, which demonstrates that no Pd (and therefore, no metallacage) is retained intracellularly, nor unspecifically bound, nor retained in the insert filter.

In previous studies, PepH3 was shown to present translocation values above 50% after 24 h incubation, reaching an equilibrium distribution across the BBB.[30] Here, we show that the conjugation of the metallacage to this peptide also leads to an increase on its translocation ability. A post-translocation integrity assay was also performed, and no decrease in the integrity of the cell model was detected, further supporting the nontoxic character of the metallacages.

**Biodistribution Studies of $^{99m}$Tc-Labeled PepH3 Exofunctionalized $[Pd_2L_4]^{4+}$ Metallacage in CD1 Mice.** Encouraged by the noteworthy translocation efficacy of the $\mathbf{C}^{\mathbf{PepH3}}$ cage in the *in vitro* BBB model, an initial biodistribution study in healthy mice using the radioactive host−guest system $[[^{99m}TcO_4]^- \subset \mathbf{C}^{\mathbf{PepH3}}]$ was performed to assess its ability to cross the BBB *in vivo*. The uniqueness of this radiolabeling approach, namely, the speed and efficacy of noncovalent encapsulation of $[^{99m}TcO_4]^-$, avoiding additional reagents, counteracting the rapid decay of the radioisotope, was previously highlighted.[29] Therefore, based on a modified procedure[29] the radioactive cage $[[^{99m}TcO_4]^- \subset \mathbf{C}^{\mathbf{PepH3}}]$ was prepared *in situ* upon addition of a $Na[^{99m}TcO_4]$ solution, eluted from a $^{99}$ Mo/$^{99m}$Tc generator using saline (0.9% sodium chloride), to a solution of $\mathbf{L}^{\mathbf{PepH3}}$ in DMSO (2 equiv), followed by addition of $[Pd(NCCH_3)_4](BF_4)_2$ (1 equiv) as a solid. After 1 h incubation at 37 °C, the radiolabeled cage $[[^{99m}TcO_4]^- \subset \mathbf{C}^{\mathbf{PepH3}}]$ was purified and isolated using a Sep-Pak C18 cartridge to remove hydrophilic impurities, mainly nonencapsulated $[^{99m}TcO_4]^-$ (ca. 37%). The column was then eluted with methanol to recover the radioactive cage. The initial fractions containing nonencapsulated $[^{99m}TcO_4]^-$ and the fractions containing the radioactive cage $[[^{99m}TcO_4]^- \subset \mathbf{C}^{\mathbf{PepH3}}]$ were monitored by instant thin layer chromatography (ITLC-SG) as described in the Experimental section (SI, Figures S11−S13). The radioactive cage $[[^{99m}TcO_4]^- \subset \mathbf{C}^{\mathbf{PepH3}}]$ was administrated intravenously via tail vein to CD1 mice ($n$ = 3) and its biodistribution evaluated at 5 min post-injection. The obtained data summarized in Table 1 clearly demonstrate that cage $[[^{99m}TcO_4]^- \subset \mathbf{C}^{\mathbf{PepH3}}]$ is able to cross the BBB, accumulating in the brain (0.42 ± 0.06% ID/g). It should be noted that the free pertechnetate's accumulation in the brain can be considered negligible.[38] Interestingly, the brain uptake of the cage is comparable to that observed for the "free" peptide PepH3 in the same animal model at the same time point (0.31 ± 0.07% ID/g).[30] This result confirms that the latter behaves as a shuttle peptide for taking cargo into the brain.


https://dx.doi.org/10.1021/acs.bioconjchem.0c00659
Bioconjugate Chem. 2021, 32, 1399−1408

**Table 1. −Biodistribution of $[[^{99m}TcO_4]^- \subset \mathbf{C}^{PepH3}]$ at 5 min p.i. in CD1 Mice[a]**

| Organ | % I.D./g |
|---|---|
| Blood | 9.0 ± 0.5 |
| **Brain** | **0.42 ± 0.06** |
| Liver | 5.4 ± 0.2 |
| Intestine | 2.3 ± 0.2 |
| Spleen | 3.6 ± 0.6 |
| Heart | 4.4 ± 1.0 |
| Lung | 5.3 ± 0.4 |
| Kidney | 4.2 ± 0.5 |
| Muscle | 1.9 ± 0.2 |
| Bone | 2.8 ± 0.4 |
| Stomach | 7.6 ± 3.3 |
| Thyroid | 9.1 ± 1.9 |

[a]Results are expressed as% I.D./g tissue (mean ± SD, $n$ = 3).

Although these values are not comparable to the ones described for the "gold standard" brain imaging agents, namely, $Tc^{99m}$-labeled hexamethyl-propyleneamine oxime and $Tc^{99m}$-ethylcysteinate dimer (ca. 3−4% ID/g at short post-injection times in mice),[39] it must be emphasized that these agents are low-molecular-weight lipophilic complexes that diffuse passively through the BBB, whereas $[[^{99m}TcO_4]^- \subset \mathbf{C}^{PepH3}]$ is a high-molecular-weight system containing a charged scaffold. Moreover, the brain accumulation of $[[^{99m}TcO_4]^- \subset \mathbf{C}^{PepH3}]$ is higher than the endogenous peptides able to cross the BBB such as the case of amylin, insulin, PYY3−36, and secretin, featuring a brain uptake between 0.045 ID/g and 0.176% ID/g after intravenous injection in the tail vein.[40−43] Other examples of known BBB peptide vectors include the CPPs peptides TAT, penetratin, synB1, and others, which present brain accumulations in the range 0.2−0.9%ID/g of tissue.[44]

Another relevant issue to be addressed relates to the stability of the radiolabeled cage *in vivo*, namely, with the possible release of encapsulated $[^{99m}TcO_4]^-$ to the bloodstream. It is known that iodide and $[^{99m}TcO_4]^-$ are avidly taken up by the sodium-iodide symporter (NIS),[45] which is endogenously expressed in high amounts in the thyroid gland, the stomach, and the salivary glands. Therefore, accumulation of activity in these specific organs/tissues is a clear indication of the presence of $[^{99m}TcO_4]^-$ in circulation. A comparative biodistribution study in mice reported by Zuckier et al. demonstrated that in the case of free $[^{99m}TcO_4]^-$ the activity in stomach was several-fold greater than in blood, and the activity in the thyroid gland almost doubled with respect to the activity found in blood (20 min post-injection).[45] On the contrary, in the case of $[[^{99m}TcO_4]^- \subset \mathbf{C}^{PepH3}]$, the activity in blood (9.0 ± 0.5% I.D./g), stomach (7.6 ± 3.3% I.D./g), and thyroid (9.1 ± 1.9 I.D./g) are comparable, which suggests that the level of free $[^{99m}TcO_4]^-$ is not very high and points out to a moderate stability of the host−guest complex *in vivo* at short time points. Of note, the previously reported biodistribution results of the cobalt pertechnetate host−guest complex have shown that the activity detected in stomach and thyroid is several-fold higher than in blood,[29] which is an indication of high levels of pertechnetate being released from the cage to blood circulation (120 min post-injection).

## CONCLUSIONS

In conclusion, we report here the synthesis of a new self-assembled cationic $[Pd_2L_4]^{4+}$ metallacage tethered to a BBB penetrating peptide. The resulting water-soluble cage $\mathbf{C}^{PepH3}$ crosses the BBB with respect to the untargeted cage $\mathbf{C}^{0}$, as demonstrated in a BBB cell model *in vitro*. Furthermore, the cage has been used as targeted delivery system of the pertechnetate ion exploiting its host−guest chemistry. Thus, *in vivo* biodistribution studies in mice of the radiolabeled host−guest $[[^{99m}TcO_4]^- \subset \mathbf{C}^{PepH3}]$ complex show that it is able to cross the BBB, being the brain accumulation higher than the one of the free peptide shuttle PepH3[30] and of other peptides designed for brain-targeted delivery. While these studies represent a proof-of-concept that is possible to target supramolecular coordination complexes and their host−guest adducts to specific organs, still further investigation and cage design are necessary to validate their applicability, including pharmacokinetic studies and optimization of the host−guest chemistry to enhance stability.

In the future, the cage scaffold could be used to enable imaging in the brain using other modalities (e.g., MRI, PET), not only exploiting noncovalent interactions within its cavity, but also via the *exo*-functionalization of the pyridyl scaffold with appropriate ligands and linkers.[46] Recently, we explored similar homoleptic $[Pd_2L_4]^{4+}$ systems *exo*-functionalizing of the ligand with fluorescent tags facilitating the study of the cages' cellular accumulation by fluorescence microscopy *in vitro*.[47−49] Furthermore, the metallacage may enable orthogonal imaging using different techniques (e.g., guest cage designed for PET, host for MRI, etc.). Similarly, the robustness and modular composition of these supramolecular metal-based structures could enable the introduction of tumor targeting moieties (e.g., peptides or antibodies). Presently, our laboratories are exploring the possibility to achieve heteroleptic cages featuring different functionalities, while encapsulating anticancer drugs (e.g., cisplatin). Brought together, the obtained results pave the way toward the development of versatile brain-targeted *theranostic* based on $[Pd_2L_4]^{4+}$ metallacages.

## EXPERIMENTAL SECTION

**General.** *Chemicals.* All reagents and solvents were obtained from commercial suppliers and used without further purification, unless otherwise stated. Triethylamine was distilled under nitrogen before use. Cage $\mathbf{C}^{0}$ was synthesized according to previously reported procedures.[25]

*NMR Spectroscopy.* $^1H$ NMR and $^{13}C\{^1H\}$-NMR, were recorded on a 500 MHz DMX (Bruker), 400 MHz AV spectrometer (Bruker), or 400 MHz Avance 400 (Bruker). Chemical shifts are given in parts per million (ppm). Abbreviations for NMR multiplicities are singlet (s), doublet (d), triplet (t), multiplet (m), and broad (b). Coupling constants $J$ are given in Hz. The following solvents were used as internal standards: MeOD: 3.31 ppm ($^1H$ NMR) and 49.00 ppm ($^{13}C$ NMR); $CDCl_3$: 7.26 ppm ($^1H$ NMR) and 77.16 ppm ($^{13}C$ NMR).[1] ESI-MS spectra were recorded on a Walter Synapt G2SI QTOF and a Bruker Daltonics Esquire 3000 plus spectrometers.

*Reverse Phase High Performance Liquid Chromatography (RP-HPLC).* HPLC analyses were performed on a PerkinElmer LC pump 200 coupled to a Shimadzu SPD 10AV UV/vis spectrometer. Analytical control and semipreparative purification of the peptides and peptide conjugates were achieved on a Supelco Discovery Bio Wide Pore C18−5 column (250 mm × 4.6 mm, 5 μm) and Supelco Discovery Bio Wide Pore C18 column (250 mm × 10 mm, 10 μm) with a flow rate of 1.0 mL $min^{-1}$ and 2.0 mL $min^{-1}$, respectively. Linear gradients of eluent A (0.1% volume/volume [v/v] TFA in water) and eluent B


https://dx.doi.org/10.1021/acs.bioconjchem.0c00659
Bioconjugate Chem. 2021, 32, 1399−1408

(0.1% [v/v] TFA in acetronitrile) were applied according to methods:

*Analytical Control.* 0−25 min, 10−50% B; 25−27 min, 100% B; 27−28 min, 100−0% B; 28−30 min, 10% B.

*Semipreparative Purification.* 0−35 min, 25−50% B; 35−37 min, 100% B; 37−41 min, 100−0% B; 41−42 min, 25% B.

**Synthesis.** *Ligand $L^0$.* The carboxylic *exo*-functionalized ligand 2-(3,5-bis(pyridin-3-ylethynyl)phenyl)acetic acid ($\mathbf{L^0}$) was synthesized following previously reported procedures.[25] In brief, the reactive carboxylic acid functional group of 3,5-dibromobenzylacetic was protected using benzyl bromide. The dibromophenyl benzoate could then be coupled to 3-ethynylpyridine under Sonogashira cross coupling conditions, before deprotection of the benzyl group via sodium hydroxide, and subsequent acidification, afforded $\mathbf{L^0}$ (see Supporting Information for characterization).

*Synthesis of PepH3-PEG-Ligand ($L^{PepH3}$) and Cage ($C^{PepH3}$).* Detailed description of the synthesis via SPPS protocols combined to self-assembly, as well as products characterization are provided in the Supporting Information.

**DFT Calculations.** The initial cage structure was adapted from CCDC 1431657 file.[24] The *endo*-functionalized central pyridyl ring of each ligand was replaced with the phenyl derivative and the *exo*-functionalization extended to the $CH_2COOH$ carboxylic structure to create the $\mathbf{C^0}$ cage. This modeling was undertaken using the Molecular Operating Environment (MOE) software.[50] Geometry optimization in the gas phase was run using Schrodinger Jaguar 10.9[51,52] with DFT-PBE0[34] functional, combined with 6-31g** (C, N, O and H) and LANL2DZ (Pd and Tc) basis sets. The combination of two basis sets has been previously shown to calculate transition metal complexes, in conjunction with a hybrid functional such as PBE0, with higher accuracy.[53]

**Encapsulation Studies of "Cold" Perrhenate and Stability toward GSH by $^1$H NMR Spectroscopy.** 2.0 mg $L^{PepH3}$ (4 equiv) was dissolved in 400 $\mu$L $D_2O$/DMSO-$d_6$ [4:1] and $^1$H NMR spectrum was recorded on a Bruker Avance III-400 US. Afterward, 0.319 mg $Pd(CH_3CN)_4(BF_4)_2$ (2 equiv) was dissolved in 25 $\mu$L of the same solvent mixture and added to the NMR tube, mixed carefully, and incubated for 30 min at room temperature. The completed cage formation was observed after 30 min by $^1$H NMR showing the characteristic downshifts of the $\alpha$-protons of the pyridine moieties. For encapsulation studies, 0.196 mg $NaReO_4$ (2 equiv) was dissolved in 25 $\mu$L of the respective solvent mixture, added to the NMR tube and mixed. $^1$H NMR spectra were recorded after 30 and 75 min incubation. For stability studies, reduced GSH (10 equiv, 1.103 mg) was added to a solution of $[[ReO_4]^- \subset \mathbf{C^{PepH3}}]$, properly mixed, and $^1$H NMR spectra recorded at different times over 24 h.

**Cell Culture.** bEnd.3 murine brain endothelioma cells (ATTCC-CRL2299) were grown in DMEM supplemented with 10% fetal bovine serum (FBS) (all from Invitrogen) in a humidified atmosphere of 95% air and 5% $CO_2$ at 37 °C (Heraeus, Germany), with the medium changed every other day. To allow the formation of a stable *in vitro* BBB model, 5000 cells per well were seeded in fibronectin-coated tissue culture PET inserts (pore size of 1 $\mu$m) for 24-well plates (BD falcon) and grown for 9 days with media changed every 2 days, as previously described.[30,37]

**Cytotoxicity Assay.** The cytotoxicity of the metallacages in the cell line under study was evaluated using a colorimetric method based on the tetrazolium salt MTT. Cells were seeded in 96-well plates at a density of $2 \times 10^4$ cells per well in 200 $\mu$L of culture medium and left to incubate overnight for optimal adherence. Stock solutions of metallacage prepared fresh in DMSO were diluted in medium, and serial dilutions were added to the wells and incubation was performed at 37 °C/5% $CO_2$ for 24 h. The percentage of DMSO in cell culture medium did not exceed 1% (except for $\mathbf{C^0}$ where 2% were present in the solution with the highest concentration). At the end of the incubation period, the compounds were removed and the cells were incubated with 200 $\mu$L of MTT solution (500 $\mu$g/mL). After 3−4 h at 37 °C/5% $CO_2$, the medium was removed, and the purple formazan crystals were dissolved in 200 $\mu$L of DMSO by shaking. The cell viability was evaluated by measurement of the absorbance at 570 nm using a plate spectrophotometer (Power Wave Xs, Bio-Tek). The cell viability was calculated by dividing the absorbance of each well by that of the control wells. Each point was determined in at least 4 replicates in 2 independent assays.

**BBB Integrity Assay.** For the evaluation of the integrity of the BBB model, fluorescein isothiocyanate-dextran with a MW of 4 (FD4 from Sigma-Aldrich) was used as a fluorescent probe, as previously described.[30,54] First, FD4 was diluted in transport medium (DMEM fluorobrite +10% FBS all from Invitrogen) to an absorbance of 0.1, from a stock of 25 mg mL$^{-1}$. Cells were washed twice with PBS and once with transport medium, and then diluted FD4 was added to the apical side, while regular transport medium was added to the basal side. Cells were incubated for 2 h at 37 °C/5% $CO_2$, and samples were then collected from the apical and basolateral sides and fluorescence intensity was measured at $\lambda$ with an excitation of 493 nm and maximum emission at 560 nm in a plate reader (TECAN infinity M200). Empty inserts (without cells) were used as a control. Only cells present in inserts with values of integrity higher than 90% were used for subsequent studies. The assay was also repeated after the translocation assay with the metallacages.

**BBB Translocation Assay.** bEnd.3 cells grown in tissue culture inserts for 9 days and with integrity values higher than 90% were used for the translocation assay. Inserts were incubated with 10 mM of $\mathbf{C^0}$ and $\mathbf{C^{PepH3}}$ in transport medium (DMEM fluorobrite +10%FBS) in the apical side for 2 and 5 h, respectively. After incubation, samples were collected and analyzed by ICP-MS for quantification of the Pd content. Control inserts with only transport media or DMSO control were also submitted to the same procedure. After the translocation assay, inserts were washed (apical and basal sides) twice with PBS and once with transport medium and a post-translocation integrity assay was performed as described above. Three experiments were performed on different days using independently grown cell cultures. For ICP-MS determination of Pd content on the apical and basal fraction, each sample was incubated for 24 h with a mixture of $HNO_3$ and HCl (1:3), diluted with ultrapure water, and analyzed on a Thermo X series spectrometer.

**Preparation of the Radioactive Host−Guest Complex $[[^{99m}TcO_4]^- \subset \mathbf{C^{PepH3}}]$.** A saline solution of $Na[^{99m}TcO_4]$ (100 $\mu$L, 97.31 MBq), eluted from a radionuclide generator (DRN 4329 Ultra-TechneKow FM Mo-99/Tc-99m generator), was added to a $\mathbf{L^{PepH3}}$ DMSO solution (100 $\mu$L, 4.80 mM), followed by addition of $[Pd(NCCH_3)_4](BF_4)_2$(2.40 mM, 0.50 equiv) in solid. After incubation at 37 °C for 1 h, the self-assembled radiolabeled cage $[[^{99m}TcO_4]^- \subset \mathbf{C^{PepH3}}]$ was purified using a Sep-Pak cartridge (C18, 360 mg, 55−105 $\mu$m, Waters). After application of the sample, the cartridge was washed with water


https://dx.doi.org/10.1021/acs.bioconjchem.0c00659
Bioconjugate Chem. 2021, 32, 1399−1408

(3 mL) to remove free Na[$^{99m}TcO_4$] (31.93 MBq) until no activity could be detected in the collected fractions as monitored using a ionization chamber. The radiolabeled cage [[$^{99m}TcO_4$]$^-$ ⊂ $\mathbf{C}^{\mathbf{PepH3}}$] was eluted with methanol and collected in different fractions (4 × 0.5 mL) until no activity could be measured in the eluting fractions. *Fraction 1*, 1.40 MBq; *Fraction 2*, 21.35 MBq; *Fraction 3*, 6.55 MBq; *Fraction 4*, 0.93 MBq. The fraction with the highest activity (*Fraction 2*) was used for the biodistribution studies after evaporation of the solvent under $N_2$ flow and the residue dissolved in distilled water (ca. 200 μL). The fractions containing nonencapsulated Na[$^{99m}TcO_4$] and the fractions containing the radioactive cage [[$^{99m}TcO_4$]$^-$ ⊂ $\mathbf{C}^{\mathbf{PepH3}}$] were monitored by instant thin layer chromatography (ITLC-SG), with methylethylketone and saline (0.9% sodium chloride) as solvents. Na[$^{99m}TcO_4$] migrates in the front of the solvent (Rf = 1) in both solvents, whereas the radioactive cage remains at the origin (Rf = 0) or in the solvent front (Rf = 1) in the case of methylethylketone or saline, respectively (Supporting Information, Figures S11−S13). Radioactivity distribution on the ITLC-SG strips (Agilent Technologies) was detected using a miniGita Star scanning device (Elysia Raytest) coupled with a Gamma BGO-V-Detector (Elysia Raytest).

**Biodistribution Studies.** All animal experiments were performed in compliance with national and European regulations for animal experimentation. The animals were housed in a temperature and humidity-controlled room with a 12 h light/12 h dark schedule and maintained on normal diet *ad libitum*. The biodistribution of the radiolabeled cage [[$^{99m}TcO_4$]$^-$ ⊂ $\mathbf{C}^{\mathbf{PepH3}}$] was evaluated in a group of 3 female CD-1 mice (randomly bred, Charles River) weighting 27−30 g each. Animals were injected intravenously with 100 μL (4.8−5.2 MBq/130−141 μCi) of the preparation via the tail vein. Mice were sacrificed by cervical dislocation at 5 min post-injection (p.i.). The injected radioactive dose and the radioactivity remaining in the animal after sacrifice were measured in a dose calibrator (Capintec CRC-15W, Ramsey, USA). Blood samples were taken by cardiac puncture at sacrifice. Brain and other main organs were then dissected, rinsed to remove excess blood, weighed, and the radioactivity measured in a gamma counter (Berthold, Germany). Biodistribution results were expressed as the average of percentage of the injected radioactivity dose per gram tissue (% I.D./g).

## ■ ASSOCIATED CONTENT

### Supporting Information

The Supporting Information is available free of charge at https://pubs.acs.org/doi/10.1021/acs.bioconjchem.0c00659.

Experimental details and compound analysis by NMR spectroscopy, ESI-MS, and HPLC, as well as results of cage stability, antiproliferative activity, and radiochemical characterization (PDF)

## ■ AUTHOR INFORMATION


### Corresponding Authors

**Filipa Mendes** − *Centro de Ciências e Tecnologias Nucleares (C2TN), Instituto Superior Técnico, 2695-066 Bobadela, LRS, Portugal; Departamento de Engenharia e Ciências Nucleares (DECN), Instituto Superior Técnico, Universidade de Lisboa, 2695-066 Bobadela, LRS, Portugal;* orcid.org/0000-0003-0646-1687; Email: fmendes@ctn.tecnico.ulisboa.pt

**João D. G. Correia** − *Centro de Ciências e Tecnologias Nucleares (C2TN), Instituto Superior Técnico, 2695-066 Bobadela, LRS, Portugal; Departamento de Engenharia e Ciências Nucleares (DECN), Instituto Superior Técnico, Universidade de Lisboa, 2695-066 Bobadela, LRS, Portugal;* orcid.org/0000-0002-7847-4906; Email: jgalamba@ctn.tecnico.ulisboa.pt

**Angela Casini** − *Department of Chemistry, Technical University of Munich, 85748 Garching bei München, Germany;* orcid.org/0000-0003-1599-9542; Email: angela.casini@tum.de

### Authors

**Ben Woods** − *Institute of Structural and Molecular Biology and Department of Biological Sciences, School of Science, Birkbeck University of London, London WC1E 7HX, United Kingdom*

**Rúben D. M. Silva** − *Centro de Ciências e Tecnologias Nucleares (C2TN), Instituto Superior Técnico, 2695-066 Bobadela, LRS, Portugal*

**Claudia Schmidt** − *Department of Chemistry, Technical University of Munich, 85748 Garching bei München, Germany*

**Darren Wragg** − *Department of Chemistry, Technical University of Munich, 85748 Garching bei München, Germany*

**Marco Cavaco** − *Instituto de Medicina Molecular João Lobo Antunes (iMM-JLA), Faculdade de Medicina, Universidade de Lisboa, 1649-028 Lisboa, Portugal;* orcid.org/0000-0002-0938-9038

**Vera Neves** − *Instituto de Medicina Molecular João Lobo Antunes (iMM-JLA), Faculdade de Medicina, Universidade de Lisboa, 1649-028 Lisboa, Portugal;* orcid.org/0000-0002-2989-7208

**Vera F. C. Ferreira** − *Centro de Ciências e Tecnologias Nucleares (C2TN), Instituto Superior Técnico, 2695-066 Bobadela, LRS, Portugal*

**Lurdes Gano** − *Centro de Ciências e Tecnologias Nucleares (C2TN), Instituto Superior Técnico, 2695-066 Bobadela, LRS, Portugal; Departamento de Engenharia e Ciências Nucleares (DECN), Instituto Superior Técnico, Universidade de Lisboa, 2695-066 Bobadela, LRS, Portugal*

**Tânia S. Morais** − *Centro de Química Estrutural and Departamento de Química e Bioquímica, Faculdade de Ciências, Universidade de Lisboa, 1749-016 Lisboa, Portugal;* orcid.org/0000-0003-0233-8243

Complete contact information is available at: https://pubs.acs.org/10.1021/acs.bioconjchem.0c00659


### Author Contributions

A.C. and J.D.G.C. conceptualized the project. A.C. and J.D.G.C. wrote the manuscript and supervised the synthesis of the ligands and cages. B.W. optimized the synthesis of ligand $L^0$ and synthesized cages $C^0$. B.W. and R.D.M.S. synthesized the bioconjugated cages, optimized the synthesis of the BBB penetrating peptide, and performed NMR experiments. T.S.M. performed NMR characterization experiments. R.D.M.S. also performed the radiolabeling procedures with [$^{99m}TcO_4$]$^-$. F.M. designed, performed, and analyzed the *in vitro* experiments. V.F.C.F. was involved in the translocation assays, while M.C. and V.N. performed the BBB integrity analysis. L.G. performed the *in vivo* experiments. C.S. performed the perrhenate encapsulation and stability studies by NMR spectroscopy. D.W. performed the DFT calculations to assess the structure of the host−guest cage-pertechnetate system. A.C. and J.D.G.C. contributed to the design of the biological experiments, cage


https://dx.doi.org/10.1021/acs.bioconjchem.0c00659
Bioconjugate Chem. 2021, 32, 1399−1408

analysis, and data interpretation. All the authors contributed to the writing of the manuscript.

### Author Contributions

[¶]B.W. and R.D.M.S. contributed equally to the work.

### Notes

The authors declare no competing financial interest.

## ■ ACKNOWLEDGMENTS

J.D.G.C., F.M., and T.S.M. thank the Portuguese Fundação para a Ciência e a Tecnologia (FCT) for grants UID/Multi/04349/2019, PTDC/QUI-NUC/30147/2017, PTDC/BTM-TEC/29256/2017, and UIDB/00100/2020. FCT is also acknowledged for the PhD fellowships to V.F.C.F (SFRH/BD/108623/2015) and M.C. (PD/BD/128281/2017). T.S.M. thanks FCT for the project CEECIND/00630/2017 (acknowledging FCT, POPH, and FSE- European Social Fund). B.W. thanks the EU Erasmus Program for providing support for a short-term scientific mission at the Universidade de Lisboa, Instituto Superior Técnico.

## ■ REFERENCES

(1) Neuwelt, E., Abbott, N. J., Abrey, L., Banks, W. A., Blakley, B., Davis, T., Engelhardt, B., Grammas, P., Nedergaard, M., Nutt, J., et al. (2008) Strategies to advance translational research into brain barriers. *Lancet Neurol. 7*, 84−96.

(2) Sandoval, K. E., and Witt, K. A. (2008) Blood-brain barrier tight junction permeability and ischemic stroke. *Neurobiol. Dis. 32*, 200−19.

(3) Neuwelt, E. A., Bauer, B., Fahlke, C., Fricker, G., Iadecola, C., Janigro, D., Leybaert, L., Molnar, Z., O'Donnell, M. E., Povlishock, J. T., et al. (2011) Engaging neuroscience to advance translational research in brain barrier biology. *Nat. Rev. Neurosci. 12*, 169−82.

(4) Patel, M. M., and Patel, B. M. (2017) Crossing the Blood-Brain Barrier: Recent Advances in Drug Delivery to the Brain. *CNS Drugs 31*, 109−133.

(5) Dong, X. (2018) Current Strategies for Brain Drug Delivery. *Theranostics 8*, 1481−1493.

(6) Tang, W., Fan, W., Lau, J., Deng, L., Shen, Z., and Chen, X. (2019) Emerging blood-brain-barrier-crossing nanotechnology for brain cancer theranostics. *Chem. Soc. Rev. 48*, 2967−3014.

(7) Haumann, R., Videira, J. C., Kaspers, G. J. L., van Vuurden, D. G., and Hulleman, E. (2020) Overview of Current Drug Delivery Methods Across the Blood-Brain Barrier for the Treatment of Primary Brain Tumors. *CNS Drugs 34*, 1121−1131.

(8) Pulgar, V. M. (2019) Transcytosis to Cross the Blood Brain Barrier, New Advancements and Challenges. *Front. Neurosci. 12*, 1019.

(9) Kristensen, M., and Brodin, B. (2017) Routes for Drug Translocation Across the Blood-Brain Barrier: Exploiting Peptides as Delivery Vectors. *J. Pharm. Sci. 106*, 2326−2334.

(10) Varnamkhasti, B. S., Jafari, S., Taghavi, F., Alaei, L., Izadi, Z., Lotfabadi, A., Dehghanian, M., Jaymand, M., Derakhshankhah, H., and Saboury, A. A. (2020) Cell-Penetrating Peptides: As a Promising Theranostics Strategy to Circumvent the Blood-Brain Barrier for CNS Diseases. *Curr. Drug Delivery 17*, 375−386.

(11) Silva, S., Almeida, A. J., and Vale, N. (2019) Combination of Cell-Penetrating Peptides with Nanoparticles for Therapeutic Application: A Review. *Biomolecules 9*, 22.

(12) Falanga, A., Lombardi, L., Galdiero, E., Genio, V. D., and Galdiero, S. (2020) The world of cell penetrating: the future of medical applications. *Future Med. Chem. 12*, 1431−1446.

(13) Kurrikoff, K., Vunk, B., and Langel, Ü. (2020) Status update in the use of cell-penetrating peptides for the delivery of macromolecular therapeutics. *Expert Opin. Biol. Ther.*, 1−10.

(14) Fujita, M., and Ogura, K. (1996) Supramolecular Self-Assembly of Macrocycles, Catenanes, and Cages through Coordination of Pyridine-Based Ligands to Transition Metals. *Bull. Chem. Soc. Jpn. 69*, 1471−1482.

(15) Davis, A. V., Yeh, R. M., and Raymond, K. N. (2002) Supramolecular assembly dynamics. *Proc. Natl. Acad. Sci. U. S. A. 99*, 4793−6.

(16) Schmitt, F., Barry, N. P., Juillerat-Jeanneret, L., and Therrien, B. (2012) Efficient photodynamic therapy of cancer using chemotherapeutic porphyrin-ruthenium metalla-cubes. *Bioorg. Med. Chem. Lett. 22*, 178−80.

(17) Ahmedova, A., Momekova, D., Yamashina, M., Shestakova, P., Momekov, G., Akita, M., and Yoshizawa, M. (2016) Anticancer Potencies of Pt(II) - and Pd(II)-linked M2L4 Coordination Capsules with Improved Selectivity. *Chem. - Asian J. 11*, 474−7.

(18) Casini, A., Woods, B., and Wenzel, M. (2017) The Promise of Self-Assembled 3D Supramolecular Coordination Complexes for Biomedical Applications. *Inorg. Chem. 56*, 14715−14729.

(19) Sepehrpour, H., Fu, W., Sun, Y., and Stang, P. J. (2019) Biomedically Relevant Self-Assembled Metallacycles and Metallacages. *J. Am. Chem. Soc. 141*, 14005−14020.

(20) Cook, T. R., Vajpayee, V., Lee, M. H., Stang, P. J., and Chi, K. W. (2013) Biomedical and biochemical applications of self-assembled metallacycles and metallacages. *Acc. Chem. Res. 46*, 2464−74.

(21) Therrien, B. (2011) Drug delivery by water-soluble organometallic cages. *Top. Curr. Chem. 319*, 35−55.

(22) Therrien, B., and Furrer, J. (2014) The Biological Side of Water-Soluble Arene Ruthenium Assemblies. *Advances in Chemistry 2014*, 1.

(23) Lewis, J. E. M., Gavey, E. L., Cameron, S. A., and Crowley, J. D. (2012) Stimuli-responsive Pd2L4 metallosupramolecular cages: towards targeted cisplatin drug delivery. *Chemical Science 3*, 778−784.

(24) Schmidt, A., Molano, V., Hollering, M., Pothig, A., Casini, A., and Kuhn, F. E. (2016) Evaluation of New Palladium Cages as Potential Delivery Systems for the Anticancer Drug Cisplatin. *Chem. - Eur. J. 22*, 2253−6.

(25) Woods, B., Wenzel, M. N., Williams, T., Thomas, S. R., Jenkins, R. L., and Casini, A. (2019) Exo-Functionalized Metallacages as Host-Guest Systems for the Anticancer Drug Cisplatin. *Front. Chem. 7*, 7.

(26) Han, J., Schmidt, A., Zhang, T., Permentier, H., Groothuis, G. M., Bischoff, R., Kuhn, F. E., Horvatovich, P., and Casini, A. (2017) Bioconjugation strategies to couple supramolecular exo-functionalized palladium cages to peptides for biomedical applications. *Chem. Commun. (Cambridge, U. K.) 53*, 1405−1408.

(27) Han, J., Rader, A. F. B., Reichart, F., Aikman, B., Wenzel, M. N., Woods, B., Weinmuller, M., Ludwig, B. S., Sturup, S., Groothuis, G. M. M., et al. (2018) Bioconjugation of Supramolecular Metallacages to Integrin Ligands for Targeted Delivery of Cisplatin. *Bioconjugate Chem. 29*, 3856−3865.

(28) Yu, G., Yu, S., Saha, M. L., Zhou, J., Cook, T. R., Yung, B. C., Chen, J., Mao, Z., Zhang, F., Zhou, Z., et al. (2018) A discrete organoplatinum(II) metallacage as a multimodality theranostic platform for cancer photochemotherapy. *Nat. Commun. 9*, 4335.

(29) Burke, B. P., Grantham, W., Burke, M. J., Nichol, G. S., Roberts, D., Renard, I., Hargreaves, R., Cawthorne, C., Archibald, S. J., and Lusby, P. J. (2018) Visualizing Kinetically Robust Co(III)4L6 Assemblies in Vivo: SPECT Imaging of the Encapsulated [(99m)Tc]-TcO4(−) Anion. *J. Am. Chem. Soc. 140*, 16877−16881.

(30) Neves, V., Aires-Da-Silva, F., Morais, M., Gano, L., Ribeiro, E., Pinto, A., Aguiar, S., Gaspar, D., Fernandes, C., Correia, J. D. G., et al. (2017) Novel Peptides Derived from Dengue Virus Capsid Protein Translocate Reversibly the Blood-Brain Barrier through a Receptor-Free Mechanism. *ACS Chem. Biol. 12*, 1257−1268.

(31) Cavaco, M., Valle, J., da Silva, R., Correia, J. D. G., Castanho, M., Andreu, D., and Neves, V. (2020) DPepH3, an Improved Peptide Shuttle for Receptor-independent Transport Across the Blood-Brain Barrier. *Curr. Pharm. Des. 26*, 1495−1506.

(32) Neves-Coelho, S., Eleuterio, R. P., Enguita, F. J., Neves, V., and Castanho, M. (2017) A New Noncanonical Anionic Peptide That Translocates a Cellular Blood-Brain Barrier Model. *Molecules 22*, 1753.

(33) Corte-Real, S., Neves, V., Canhão, P., Outeiro, T. F., Castanho, M., Silva, F., and Oliveira, S. R. Antibody Molecules and Peptide Delivery Systems for use in Alzheimer's Disease and Related Disorders. WO 2016/120843, August 4, 2016.



https://dx.doi.org/10.1021/acs.bioconjchem.0c00659
*Bioconjugate Chem.* 2021, 32, 1399−1408

(34) Perdew, J. P., Ernzerhof, M., and Burke, K. (1996) Rationale for mixing exact exchange with density functional approximations. *J. Chem. Phys. 105*, 9982−9985.
(35) Biovia, D. S. (2016) *Discovery Studio Modeling Environment*, Dassault Systèmes, San Diego.
(36) Helms, H. C., Abbott, N. J., Burek, M., Cecchelli, R., Couraud, P. O., Deli, M. A., Forster, C., Galla, H. J., Romero, I. A., Shusta, E. V., et al. (2016) In vitro models of the blood-brain barrier: An overview of commonly used brain endothelial cell culture models and guidelines for their use. *J. Cereb. Blood Flow Metab. 36*, 862−90.
(37) Li, G., Simon, M. J., Cancel, L. M., Shi, Z. D., Ji, X., Tarbell, J. M., Morrison, B., 3rd, and Fu, B. M. (2010) Permeability of endothelial and astrocyte cocultures: in vitro blood-brain barrier models for drug delivery studies. *Ann. Biomed. Eng. 38*, 2499−511.
(38) Boros, E., and Packard, A. B. (2019) Radioactive Transition Metals for Imaging and Therapy. *Chem. Rev. 119*, 870−901.
(39) Apostolova, I., Wunder, A., Dirnagl, U., Michel, R., Stemmer, N., Lukas, M., Derlin, T., Gregor-Mamoudou, B., Goldschmidt, J., Brenner, W., et al. (2012) Brain perfusion SPECT in the mouse: normal pattern according to gender and age. *NeuroImage 63*, 1807−17.
(40) Banks, W. A., Kastin, A. J., Maness, L. M., Huang, W., and Jaspan, J. B. (1995) Permeability of the blood-brain barrier to amylin. *Life Sci. 57*, 1993−2001.
(41) Banks, W. A., Jaspan, J. B., Huang, W., and Kastin, A. J. (1997) Transport of insulin across the blood-brain barrier: saturability at euglycemic doses of insulin. *Peptides 18*, 1423−9.
(42) Banks, W. A., Goulet, M., Rusche, J. R., Niehoff, M. L., and Boismenu, R. (2002) Differential transport of a secretin analog across the blood-brain and blood-cerebrospinal fluid barriers of the mouse. *J. Pharmacol. Exp. Ther. 302*, 1062−9.
(43) Nonaka, N., Shioda, S., Niehoff, M. L., and Banks, W. A. (2003) Characterization of blood-brain barrier permeability to PYY3−36 in the mouse. *J. Pharmacol. Exp. Ther. 306*, 948−53.
(44) Sarko, D., Beijer, B., Garcia Boy, R., Nothelfer, E. M., Leotta, K., Eisenhut, M., Altmann, A., Haberkorn, U., and Mier, W. (2010) The pharmacokinetics of cell-penetrating peptides. *Mol. Pharmaceutics 7*, 2224−31.
(45) Zuckier, L. S., Dohan, O., Li, Y., Chang, C. J., Carrasco, N., and Dadachova, E. (2004) Kinetics of perrhenate uptake and comparative biodistribution of perrhenate, pertechnetate, and iodide by NaI symporter-expressing tissues in vivo. *J. Nucl. Med. 45*, 500−7.
(46) Meier-Menches, S. M., and Casini, A. (2020) Design Strategies and Medicinal Applications of Metal-Peptidic Bioconjugates. *Bioconjugate Chem. 31*, 1279−1288.
(47) Schmidt, A., Hollering, M., Drees, M., Casini, A., and Kuhn, F. E. (2016) Supramolecular exo-functionalized palladium cages: fluorescent properties and biological activity. *Dalton Trans 45*, 8556−65.
(48) Schmidt, A., Hollering, M., Han, J., Casini, A., and Kuhn, F. E. (2016) Self-assembly of highly luminescent heteronuclear coordination cages. *Dalton Trans 45*, 12297−300.
(49) Woods, B., Dollerer, D., Aikman, B., Wenzel, M. N., Sayers, E. J., Kuhn, F. E., Jones, A. T., and Casini, A. (2019) Highly luminescent metallacages featuring bispyridyl ligands functionalised with BODIPY for imaging in cancer cells. *J. Inorg. Biochem. 199*, 110781.
(50) *Molecular Operating Environment (MOE)*, ver. 2019.01; Chemical Computing Group ULC Montreal, Canada, 2020.
(51) Bochevarov, A. D., Harder, E., Hughes, T. F., Greenwood, J. R., Braden, D. A., Philipp, D. M., Rinaldo, D., Halls, M. D., Zhang, J., and Friesner, R. A. (2013) Jaguar: A high-performance quantum chemistry software program with strengths in life and materials sciences. *Int. J. Quantum Chem. 113*, 2110−2142.
(52) *Jaguar, ver. 10.9*, Schrodinger LLC, New York, NY, 2020.
(53) Yang, Y., Weaver, M. N., and Merz, K. M. (2009) Assessment of the "6-31+G** + LANL2DZ" Mixed Basis Set Coupled with Density Functional Theory Methods and the Effective Core Potential: Prediction of Heats of Formation and Ionization Potentials for First-Row-Transition-Metal Complexes. *J. Phys. Chem. A 113*, 9843−9851.
(54) Cavaco, M., Perez-Peinado, C., Valle, J., Silva, R. D. M., Correia, J. D. G., Andreu, D., Castanho, M., and Neves, V. (2020) To What Extent Do Fluorophores Bias the Biological Activity of Peptides? A Practical Approach Using Membrane-Active Peptides as Models. *Front. Bioeng. Biotechnol. 8*, 552035.


https://dx.doi.org/10.1021/acs.bioconjchem.0c00659
*Bioconjugate Chem.* 2021, 32, 1399−1408